IET Science, Measurement and Technology

Research Article

IET Journals
The Institution of Engineering and Technology

Strategies for two-dimensional and three-dimensional field computation in the design of permanent magnet motors

ISSN 1751-8822
Received on 27th June 2014
Accepted on 15th December 2014
doi: 10.1049/iet-smt.2014.0189
www.ietdl.org

Rafal Marek Wojciechowski[1], Cezary Jedryczka[1], Andrzej Demenko[1], Jan K. Sykulski[2] ✉

[1]*IEEE, Poznan University of Technology, ul. Piotrowo 3a, 60-965 Poznań, Poland*
[2]*School of Electronics and Computer Science, University of Southampton, Southampton SO17 1BJ, UK*
✉ *E-mail: jks@soton.ac.uk*

Abstract: This study discusses strategies for the design of permanent magnet motors (PMMs) exploiting two-dimensional (2D) and 3D field models. Five most common methodologies are compared and errors arising from 2D classical models considered. Examples comparing 2D and 3D results are presented and discussed for two selected types of motors. An approach has been put forward which allows the accuracy of classical 2D models to be improved by introducing correction coefficients arising from preliminary 3D simulations. A possibility of employing quasi-3D models has also been explored for the design and analysis of PMMs with the stator and rotor lamination packets of different lengths. Comparative analysis of results has been provided arising from the 2D and 3D models for a classical and a double rotor PMM.

1 Introduction

Contemporary design and optimisation of permanent magnet motors (PMM) usually incorporate field models – to achieve desired accuracy – typically using commercial packages based on the finite element formulation. Immediately, the designer is faced with an important decision whether to use the more accurate, but computationally complex and time-consuming three-dimensional (3D) simulation or simpler and more efficient, but less accurate, 2D modelling. When creating 2D models, symmetries are exploited and components of the field are neglected which have little or no influence on the main characteristics of the machine. For example, 2D models of the classical machines normally ignore the end connections of the windings, whereas the magnetic field only in the cross-section of the main core is considered. It should be noted, however, that this simplification may not work if the machine is short and broad. Moreover, the 2D treatment may not capture correctly all the subtleties of the field in the case of singly and doubly connected regions with induced currents, for example, in the starting cage of a line-start permanent magnet synchronous motor. Another drawback of 2D models is their inability to account for different lengths of the lamination packets of the stator and the rotor. This raises the question of how accurate 2D modelling really is.

The authors of this paper have been comparing 2D and 3D modelling for some time with the purpose of establishing the applicability of different models in the simulation, design and optimisation of electromechanical devices. In particular, ways of predicting the expected differences between 2D and 3D modelling have been sought; such a priori assessments may often be misleading and unreliable, thus a more thorough analysis is required. To improve the accuracy of 2D results, the authors propose to use correction coefficients which may be established by preliminary 3D simulations. In the case of an analysis of motors where the lengths of the stator and rotor lamination packets are different, a quasi-3D model appears to be the best approach; some comparative analysis against a full 3D solution is included later in this paper.

2 Strategies for PMM design using field models

Methodologies for the design of permanent magnet machines evolved alongside the advances in computers and numerical techniques. Currently, five different strategies may be identified, as illustrated in Fig. 1. The most common approach relies exclusively on 2D modelling (Path I) [1, 2], motivated by relative simplicity and economy of computation. Using a 2D model, it is implicitly assumed that no flux travels in a particular direction, for example, along the z-axis, and thus one of the components of the magnetic flux density is negligible, B_z in this case. Moreover, in the classical approach it is implied that the lengths of all finite elements in the direction perpendicular to the 2D surface under consideration are the same, here assumed to be equal to l_{2D}. As an example, Fig. 2 shows a 9-edge element (prism) and how it can be collapsed into a 2D representation; in consequence the edge element formulation in 3D becomes a nodal formulation in 2D for a particular component of the vector potential. Finally, some designers use both models sequentially by following up 2D computation with 3D verification of the results (Path II).

Classical 2D models must not be used for machines where the lengths of the rotor and the stator are different or magnets are skewed [3, 4]. Field distributions are fully 3D in such cases and require full 3D models. Notwithstanding, in order to avoid time-consuming 3D calculations, some designers employ simplified 2.5D or quasi-3D models (Path III). The quasi-3D models can be applied to machines of different stator and rotor lengths and where the magnetic field in one direction may either be neglected or treated approximately [5]. For illustrative purposes, consider a PM motor where the rotor is longer than the stator (Fig. 3). A 2D model assumes equal length of the rotor and the stator and designers using commercial software are often unaware of the error introduced, thinking erroneously that as the computation is performed per unit length the difference between lamination packet lengths does not matter. A quasi-3D model is a better approach in this case; the magnetic flux in the axial direction is neglected as in the 2D model, with only two components of flux density and one component of current density present. The difference, however, is because of the way in which the air-gap between the stator and the rotor is represented where a transition between elements of different lengths l occurs, where $l = l(x, y)$ as shown in Fig. 3. When creating a discrete model of this transitional region it is possible to apply the simplification similar to that of Fig. 2, bearing in mind that the edges in the gap have different lengths. As a result, when using vector potential formulation, a quasi-3D model similar to that of Fig. 2 is derived,

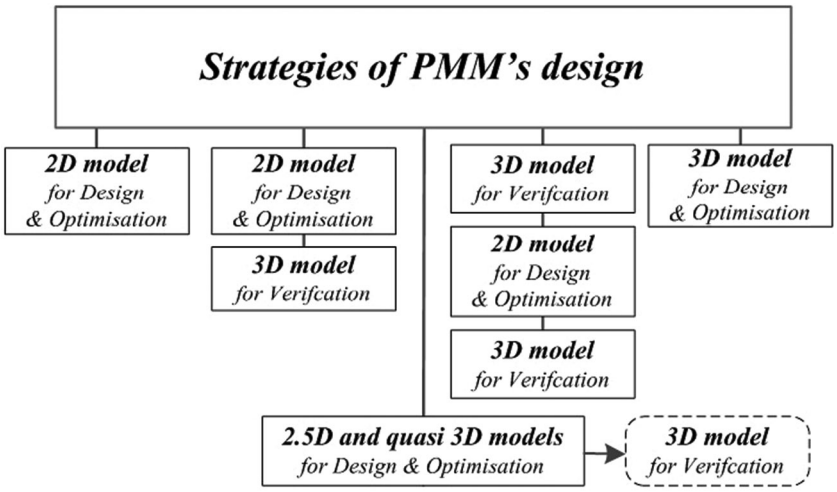

Fig. 1 *Strategies for PMM design using field models*

in which the reluctances, for example, $R_{\mu,1,1}$, depend on the difference between the stator and rotor lengths.

The 2.5D models, also known as multi-slice or multi-layer, are usually applied to machines with skewed magnets or stator slots. The formulation relies on 'slicing' the region, where individually the field is treated as 2D, and then 'stitching' them together with some conditions on flux continuity. The 2.5D approach is well known and often used [4, 6].

Path IV assumes a sequential 3D → 2D → 3D approach. Preliminary 3D simulations allow introduction of correction coefficients (e.g. equivalent length of the lamination of the motor) to be then used in design optimisation based on 2D simulation [7]. This approach is universal and allows the designer to learn more about the device being optimised, in particular study the sensitivity of the change of parameters on the characteristics, prior to the actual design, whereas the 2D model can be made more reliable. The 2D results can ultimately be verified using a 3D model. The approach may also be used for 'fine tuning' of 2.5D and quasi-3D results.

The final strategy, Path V in Fig. 1, utilises a full 3D model all along, which may have to be used – because of lack of appropriate symmetry – should the 2D, 2.5D or quasi-3D models fail to deliver sufficient accuracy [8, 9]. Unfortunately, the heavy computational burden of 3D simulation often makes this approach simply impractical.

3 Comparison of 2D classical and 3D models

To illustrate how easy it is to underestimate the errors associated with 2D treatment of 3D fields, a comparative analysis has been conducted for two selected types of machines: (a) a surface

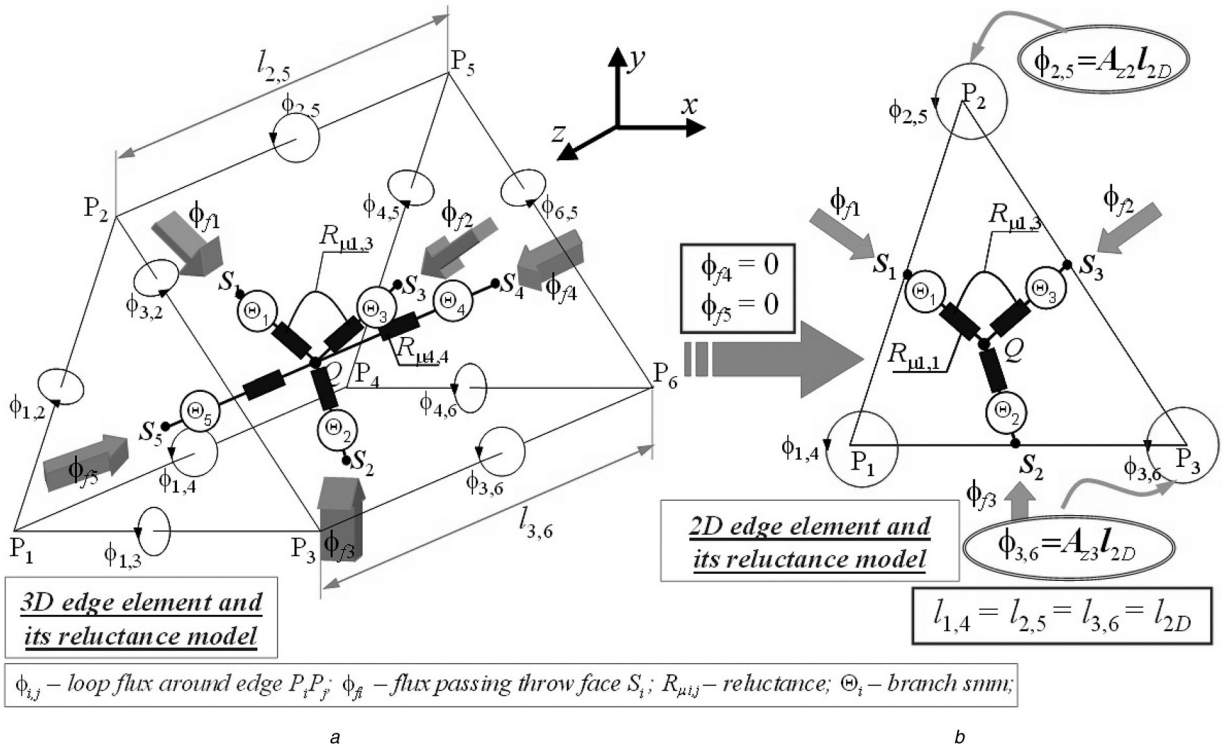

Fig. 2 *9-Edge element (prism)*

a Reluctance model of 3D edge element
b Its 2D representation

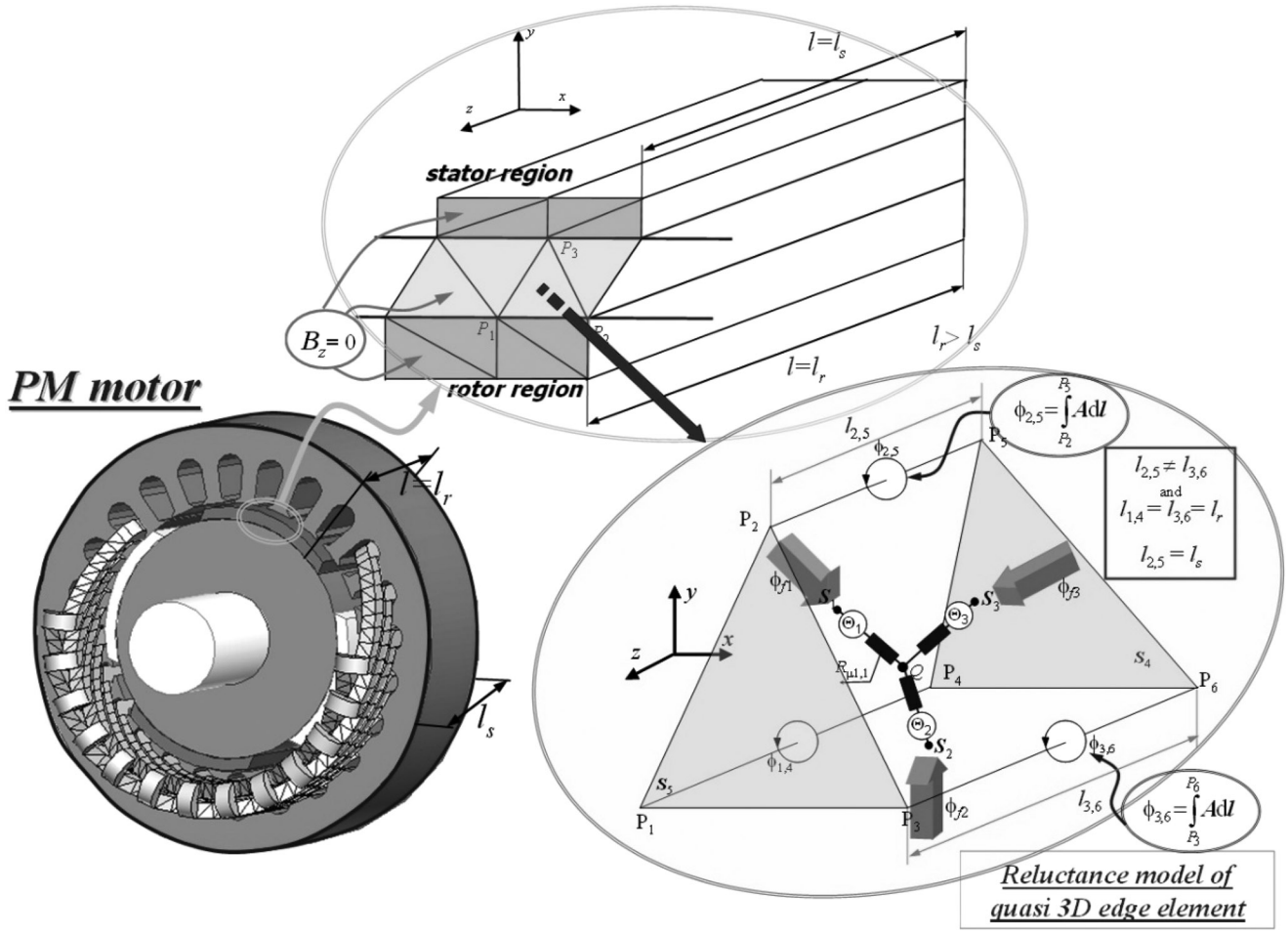

Fig. 3 *Air-gap representation when stator and rotor are of different lengths*

permanent magnet (SPM) motor, with magnets fixed to the outside of the rotor back iron [10] and (b) a PMM with twin cylindrical rotors (PMTCR) and Gramme ring winding [11], as shown in Fig. 4. The ratings and prime parameters of the two motors are summarised in Table 1. Both motors have been designed and analysed; the construction of the SPM is well known and often considered with a 2D model used commonly by most designers. The PMTCR motor offers some symmetries; notwithstanding a full 3D model seems more appropriate.

For the electromagnetic field computation, an in-house dedicated software package has been used based on the edge formulation in terms of the vector potential, for both 2D and 3D analyses in the PM machines, where the equations describe the edge values ϕ of the potential $\boldsymbol{A}$. It was shown in [12] that the edge element equations in terms of $\boldsymbol{A}$ are equivalent to loop equations of the reluctance network (RN). The total number of equations for the SPM motor – where half of the motor was meshed – was 44 283 for 2D and over 450 000 for 3D, whereas for the PMTCR motor – where because of symmetry only 1/8 of the machine had to be modelled – the respective figures were 17 280 and over 580 000 (the numbers quoted for the 3D models refer to motors of nominal dimensions). For both 2D and 3D edge formulations, the equations may be written as

$$\boldsymbol{k}_e^T \boldsymbol{R}_\mu \boldsymbol{k}_e \boldsymbol{\phi} = \boldsymbol{k}_e^T \boldsymbol{\Theta} \tag{1}$$

where $\boldsymbol{R}_\mu$ is the matrix of branch reluctances of RN (see Fig. 2), $\boldsymbol{k}_e$ is the transposed loop matrix of RN for 2D or 3D and $\boldsymbol{\Theta}$ represents the vector of branch magnetomotive forces (mmfs). In the two cases considered here, the vector $\boldsymbol{\Theta}$ may comprise two types of components: (a) $\boldsymbol{\Theta}_m$ related to branch mmfs in the regions containing permanent magnets and (b) $\boldsymbol{\Theta}_0$ describing branch mmfs because of currents in windings. When describing sources, the electric vector potentials were used, $\boldsymbol{T}_m$ and $\boldsymbol{T}_0$, where $\boldsymbol{T}_m$ is the magnetisation vector of permanent magnets, whereas $\boldsymbol{T}_0$ describes the conduction field of currents in windings made of thin wires. Details about how to establish the components $\boldsymbol{\Theta}_m$ and $\boldsymbol{\Theta}_0$ for 2D and 3D formulations may be found in [12–14] and will not be repeated here. Instead the procedure for finding the reluctance $R_{\mu,i,j}$ will be explained. The reluctance may be calculated using the following integral

$$R_{\mu,i,j} = \int_{V_e} \boldsymbol{w}_{si}^{\mathrm{T}} \boldsymbol{\nu} \boldsymbol{w}_{sj} \, dv \tag{2}$$

where $\boldsymbol{w}_{si}$ and $\boldsymbol{w}_{sj}$ are facet functions of $\boldsymbol{S}_i$ and $\boldsymbol{S}_j$, V_e is the element volume and ν is a tensor describing the reluctivity of the medium. In the actual algorithm, an approximation of (2) has been used by applying the formula

$$\iiint_{V_e} f_e(x, y, z) \, dV = \frac{V_e}{n_w} \sum_{i=1}^{n_w} f_e(P_i) \tag{3}$$

in which n_w is the number of nodes of element P_i and $f_e(P_i)$ is the integrand at the node P_i. This expression has been successfully used to determine the relevant coefficients for both the 3D and 2D models [15], as well as for the quasi-3D models. The algorithm developed allows for the calculation of the electromagnetic torque and electromotive force (emf). It is then possible to derive relationships of the dependence of the torque and emf on time or rotor position angle. The electromagnetic torque was

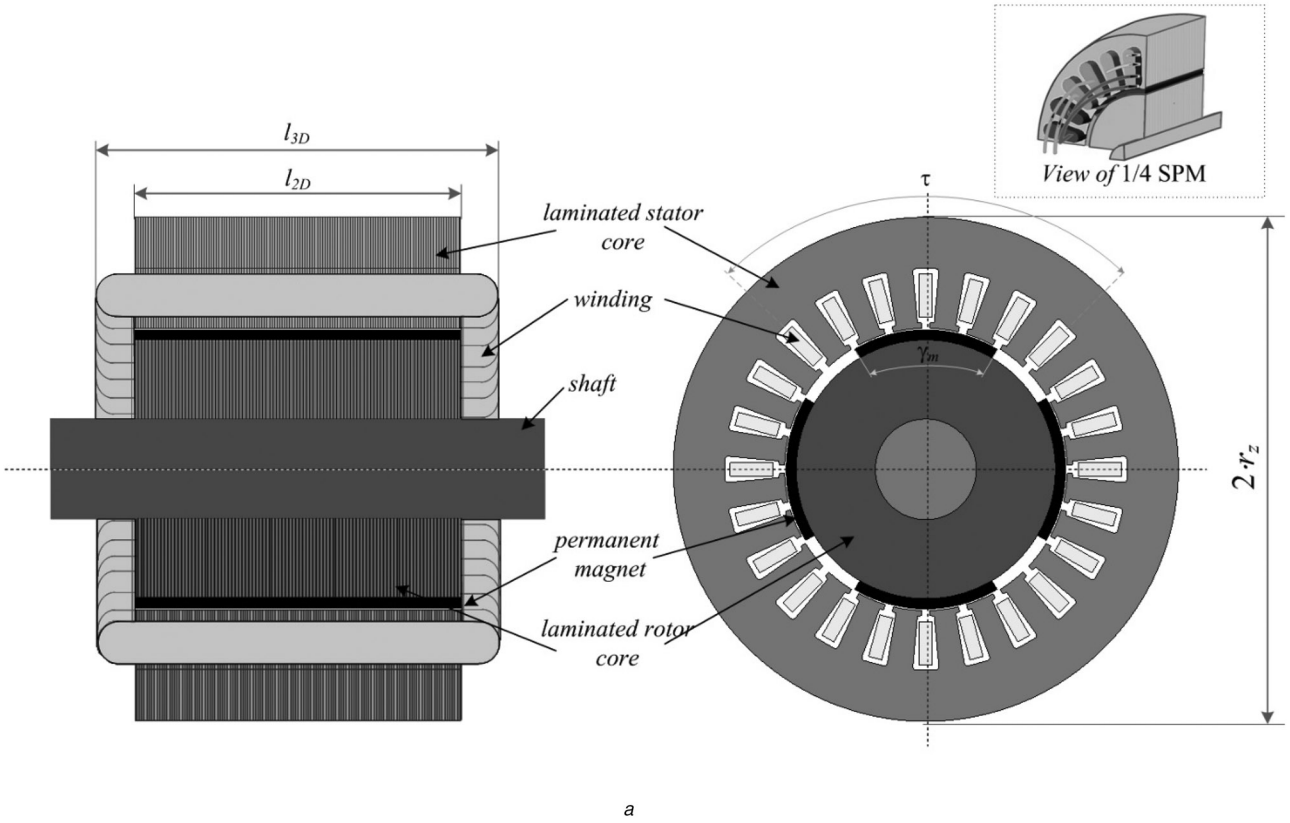

Fig. 4 *View of motor construction of:*

a SPM type
b PMTCR type

established using the Maxwell tensor method [16], whereas 'emfs' in the windings wound with thin wires used a formula presented in [12, 14].

In this paper, a comparison of 2D against 3D characteristics has been undertaken and selected results will be presented. The electromagnetic torque has been analysed in the time domain

Table 1 Ratings and main dimensions of the two motors analysed in Section 3

Parameter	SPM motor	PMTCR motor
rated power P_n, kW	0.95	18.5
rated speed n_n, rpm	1500	822
supply voltage U_{rms}, V	64	500
frequency f, Hz	50	109.6
RMS current I_{rms}, A	9.8	24
number of poles p [–]	4	16
efficiency η, %	0.89	0.91
external motor radius r_z, mm	75	170
lamination packet length l_{2D}, mm	50	165
slot pitch region τ, °	90	22.5
magnet angular width γ_m, °	61.5	20

when motors have been supplied with three-phase system of sinusoidal currents of $I_{rms} = 9.8$ A for the SPM motor and $I_{rms} = 24$ A for the PMTCR motor at a torque angle of $\delta = 90°$. Fig. 5 shows the difference ε_T between the results for the average torque obtained from 3D and 2D analyses $\{\varepsilon_T = (T_{3D} - T_{2D})/T_{3D} \cdot 100\%\}$ as a function of the ratio of the length l_{2D} of the packet of laminations to the external radius r_z of motor (see Fig. 4), for the range $0.166 \cdot r_z < l_{2D} < 3 \cdot r_z$. Fig. 6 presents the dependence of the difference ε_T on the ratio of the angular width of the magnet γ_m to the pole pitch τ. The difference has been calculated for $l_{2D}/r_z = 1$.

Another comparison, in Fig. 7, looks at the emf under light running conditions of both motors. The difference ε_{emf} between 3D and 2D results $\{\varepsilon_{emf} = (e_{3D} - e_{2D})/e_{3D} \cdot 100\%\}$ is again

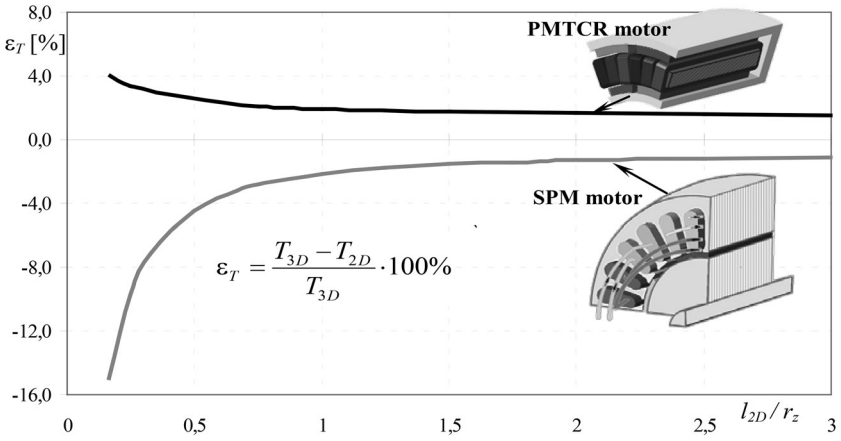

Fig. 5 *Difference between 3D and 2D calculations of the torque, for two types of motors, as a function of l_{2D}/r_z*

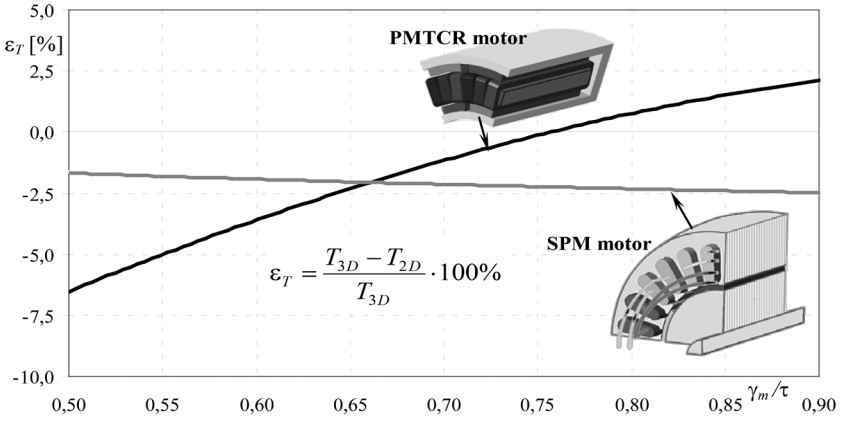

Fig. 6 *Difference between 3D and 2D calculations of the torque, for the two types of motors, as a function of γ_m/τ*

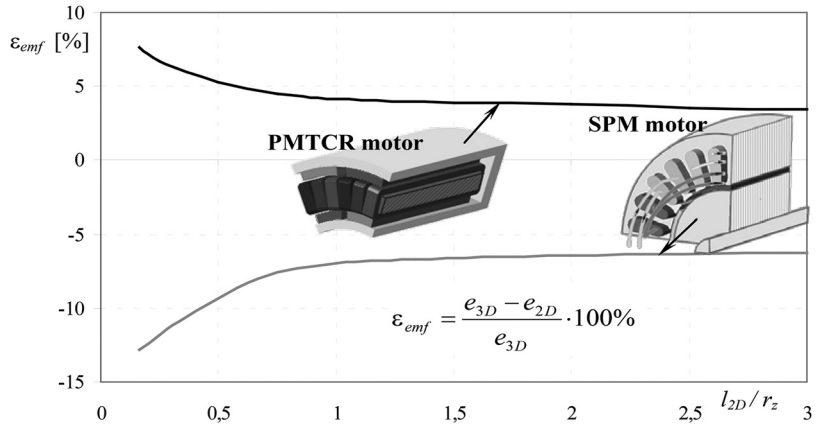

Fig. 7 *Difference between 3D and 2D calculations of the first harmonic of emf for two types of motors*

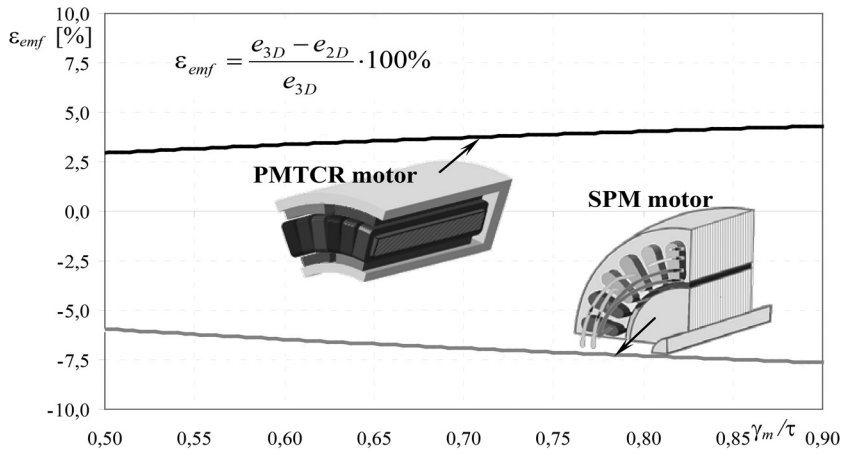

Fig. 8 *Difference between 3D and 2D calculations of the first harmonic of emf as a function of γ_m/τ*

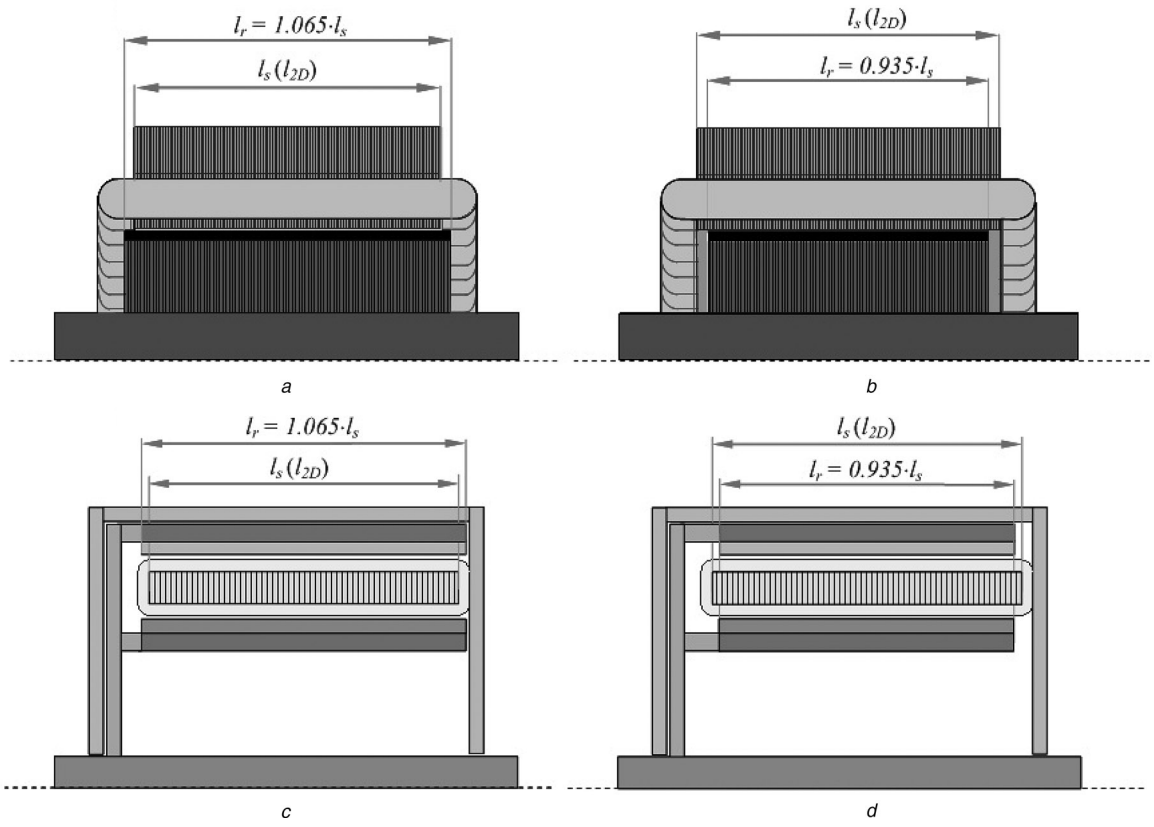

Fig. 9 *Motor construction of*

a SPM with longer rotor, $l_r > l_s$
b SPM with shorter rotor, $l_r < l_s$
c PMTCR with longer rotor, $l_r > l_s$
d PMTCR with shorter rotor, $l_r < l_s$

expressed in terms of the ratio $l_{2D}/r_z = 1$, for different ratios of γ_m/τ, that is the width γ_m of the magnet to the pole pitch τ (see Fig. 8).

An attempt was made to fit analytical functions into the computed results. For example, for the SPM motor the curve from Fig. 5 was approximated using the function $\varepsilon_T = -2.45 \cdot (l_{2D}/r_z)^{-0.925}$, which was then incorporated into a design procedure based on 2D modelling by adding a correcting coefficient. The particularly encouraging outcome was an observation that after this correction has been applied the resultant torque in the range $l_{2D} \in (0.166 \cdot r_z, 3 \cdot r_z)$ was within 1.3% (at worst) of the values obtained from full 3D analysis. A similar treatment has been applied to the first harmonic of the 'emf' computed using a 2D model of the PMTCR

Table 2 Relative differences ε_T between average torques and ε_{emf} between the first harmonics of the 'emf' obtained from 2D and quasi-3D modelling

	Classical 2D model		Quasi-3D model	
	ε_T, %	ε_{emf}, %	ε_T, %	ε_{emf}, %
SPM motor with longer rotor	1.62	1.56	−0.12	0.49
SPM motor with shorter rotor	−8.93	−10.23	−1.36	−1.04
PMTCR motor with longer rotor	2.72	5.18	−1.56	1.03
PMTCR motor with shorter rotor	−7.15	−7.33	−1.73	−1.67

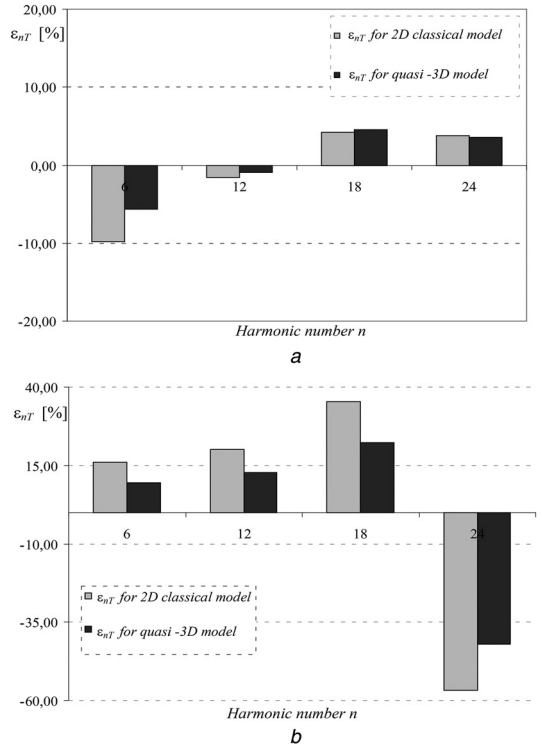

Fig. 10 *Differences ε_{nT} between the nth harmonic of the function T(α) for motor of*

a SPM
b PMTCR, both with the longer rotors, $l_r > l_s$

motor. It was found that the relationship between the difference ε_{emf} and the ratio of the average length of a single turn in the 3D model l_{w_3D} and the length l_{2D} in the 2D model may be expressed as $\varepsilon_{\text{emf}} = 3.48 \cdot \left(l_{w\_3D}/l_{2D}\right)$. It should be noted that the above correction functions are provided for illustrative purpose only. In the case of the design or performance analysis of a particular motor, a data set of values of ε_i should be created describing the relationships between parameters – such as torque, power, losses, currents etc. – for the selected proportions of dimensions, but also different technologies and/or material properties, as discussed, for example, in [7]. Such a database of differences should be established individually at the outset of the design process.

The results for the PMTCR motor were somewhat surprising although. It was anticipated that because of the winding design (the Gramme winding type) and two-level arrangement of the magnets, the differences between results of 2D and 3D analysis would be bigger than those obtained from the comparative analysis. These smaller than expected differences are likely to have resulted from weaker end effects in the PMTCR motor than in the SPM motor, but may also be due to the fact that PMTCR has a smooth (toothless) stator and a large air-gap between the magnetic cores of the stator and the rotor, thus leading to smaller harmonic content in the air-gap flux waveform created by the permanent magnets.

4 Comparison of 2D classical against quasi-3D models

In the authors' opinion in the case of PM motors of different stator and rotor lengths, the most promising approach is to use a

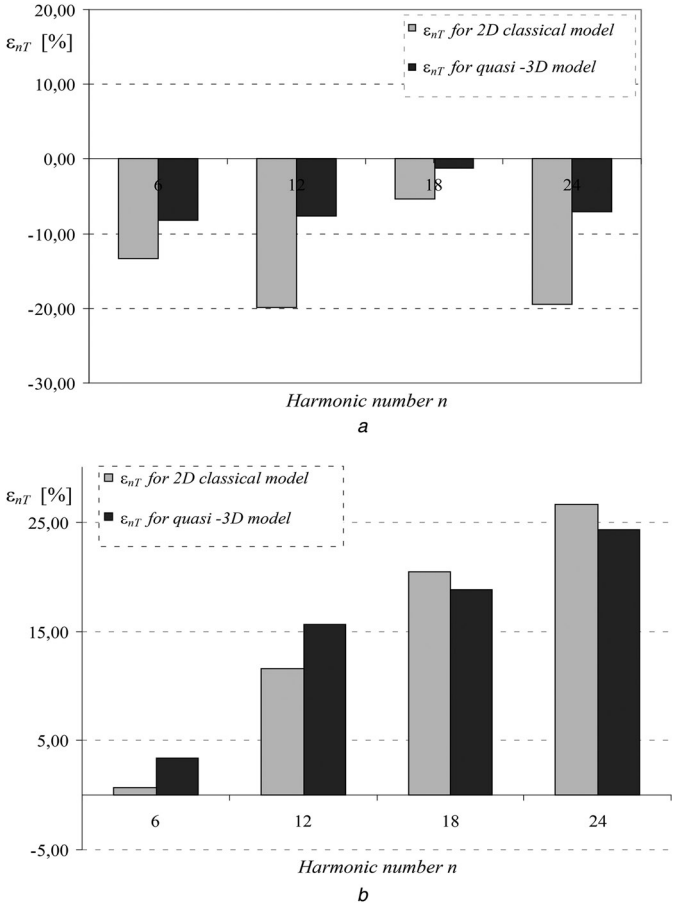

Fig. 11 *Differences ε_{nT} between the nth harmonic of the function T(α) for motor of*

a SPM
b PMTCR, both with the longer stator, $l_s > l_r$

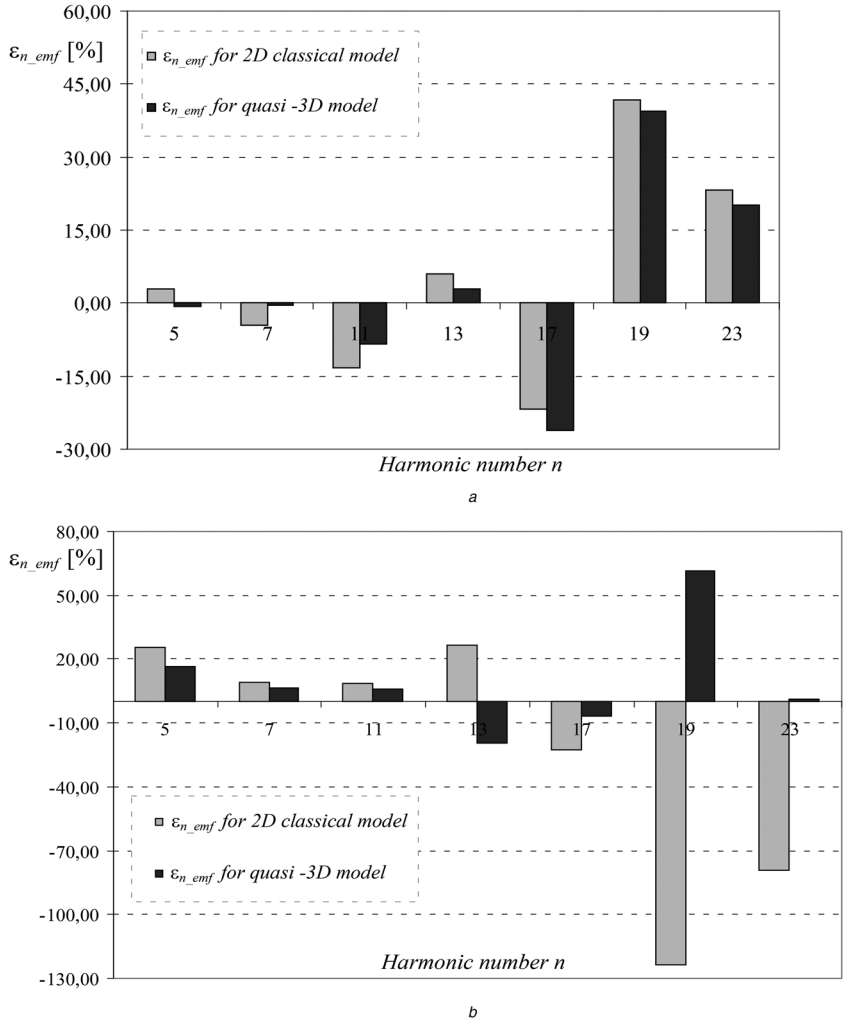

Fig. 12 *Differences $\varepsilon_{n\_\mathrm{emf}}$ between the n-harmonics of the waveform emf for motor of*
a SPM
b PMTCR, both with the longer rotors, $l_r > l_s$

quasi-3D model as depicted in Fig. 3. To substantiate this recommendation, a comparative analysis has been conducted for the two motors SPM and PMTCR with the ratio $l_{2D}/r_z = 0.5$ where the rotors have been: (a) prolonged by 6.5% (Figs. 9*a* and *c*) and (b) shortened by 6.5% (Figs. 9*b* and *d*). Both 2D and quasi-3D models were attempted and results compared with a full 3D analysis; for the 2D case, the assumption was made of the stator and rotor to be of equal lengths and equal to the length of the stator l_s (Fig. 9). The edge element formulation and setting up of the matrix $\boldsymbol{R}_\mu$ were described in Section 3.

The comparative analysis is focused on the torque and 'emf' characteristics. In torque calculations, a sinusoidal current in the windings was assumed of a known root-mean-square (RMS) value (assumed to be 9.8 A for the SPM motor and 24 A for the PMTCR motor). The 3D results were taken as a benchmark with which 2D and quasi-3D results were compared. Table 2 summarises the differences ε_T and $\varepsilon_{\mathrm{emf}}$ between computed torque and fundamental harmonic of the 'emf' for the motors with elongated and shortened rotors. The differences ε_{nT} and $\varepsilon_{n\_\mathrm{emf}}$ related to higher harmonics of the torque as a function of the rotor position $T(\alpha)$, as well as the 'emf' shape at light running, have also been considered. The differences ε_{nT} for the *n*th harmonic of the torque $T(\alpha)$ have been calculated from

$$\varepsilon_{nT} = \frac{T_{n\_3\mathrm{D}} - T_{n\_2\mathrm{D}}}{T_{n\_3\mathrm{D}}} \cdot 100\% \quad \text{for 2D models} \tag{4a}$$

and

$$\varepsilon_{nT} = \frac{T_{n\_3\mathrm{D}} - T_{n\_q3\mathrm{D}}}{T_{n\_3\mathrm{D}}} \cdot 100\% \quad \text{for quasi} - \text{3D models} \tag{4b}$$

whereas the differences $\varepsilon_{n\_\mathrm{emf}}$ for the *n*th harmonic of the 'emf' from

$$\varepsilon_{n\_\mathrm{emf}} = \frac{e_{n\_3\mathrm{D}} - e_{n\_2\mathrm{D}}}{e_{n\_3\mathrm{D}}} \cdot 100\% \quad \text{for 2D models} \tag{5a}$$

and

$$\varepsilon_{n\_\mathrm{emf}} = \frac{e_{n\_3\mathrm{D}} - e_{n\_q3\mathrm{D}}}{e_{n\_3\mathrm{D}}} \cdot 100\% \quad \text{for quasi} - \text{3D models} \tag{5b}$$

where $T_{n\_3\mathrm{D}}$, $T_{n\_2\mathrm{D}}$, $T_{n\_q3\mathrm{D}}$ and $e_{n\_3\mathrm{D}}$, $e_{n\_2\mathrm{D}}$, $e_{n\_q3\mathrm{D}}$ represent the differences in the *n*th harmonic of the torque or emf, respectively, for the 3D, 2D and quasi-3D models. The calculated differences ε_{nT} and $\varepsilon_{n\_\mathrm{emf}}$ are shown in Figs. 10–13.

The results for both motors at various core lengths of the stator and the rotor indicate that the quasi-3D approach is more accurate than 2D and yields results closer to the full 3D analysis. The 'worst' improvement was two-fold for the case of the PMTCR motor with a longer rotor; all other cases resulted in even better accuracy. Perhaps this was to be expected intuitively, but having some quantitative assessment is hoped to be more convincing.

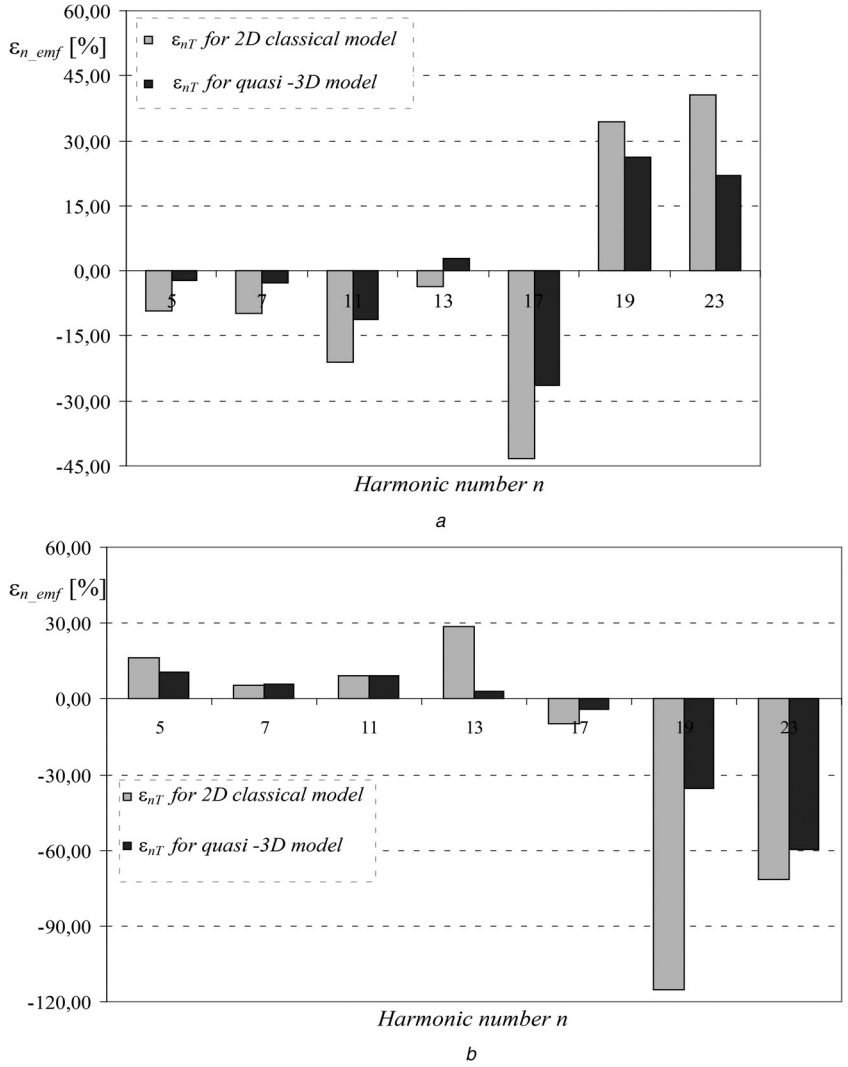

Fig. 13 *Differences* $\varepsilon_{n\_\mathrm{emf}}$ *between the harmonics of the waveform emf for motor of*
a SPM
b PMTCR, both with a longer stator, $l_s > l_r$

Finally, magnetic saturation was also considered and it was concluded that there was very little impact of the magnetic saturation on the performance characteristics of these types of machines; this was in fact expected as a consequence of a large air gap and the relative permeability of the permanent magnets being close to unity – a common feature of contemporary permanent magnet machines. Thus, although not completely negligible, the effect of saturation was found to be marginal; consequently, no particular results have been included here as they do not add any useful information to the treatment.

5 Conclusions

In the paper, different strategies for exploiting 2D, quasi-3D and 3D field modelling for the design and analysis of the PMMs have been discussed. It has been demonstrated, using particular examples that the a priori assessment of the accuracy of 2D modelling is difficult and may be unreliable. The accuracy of the 2D simulation is influenced not only by the slenderness of the machine, which is a common view, but also by the actual distribution of sources, dimensional proportions and properties of materials, as had been observed before [7]. Thus the initial assessment of the machine may often be incorrect. It is the authors' opinion that in the design process of permanent machines the most reliable is Path IV, where the main design optimisation is based on a 2D model, which is ultimately verified by a 3D simulation, but prior to the design stage relevant correction coefficients are introduced (such as described in [7, 17]) also utilising 3D models. Finally, it has been pointed out that using quasi-3D models leads to improved accuracy in cases where stator and rotor are of different lengths.

6 Acknowledgment

This research effort is carried out by the research project under agreement number 04/42/DS PB/0161.

7 References

1 Petkovska, L., Lefley, P., Cvetkovski, G.: 'Synthesis and analysis of a high-performance low-cost permanent magnet brushless DC motor', *COMPEL*, 2012, **31**, (5), pp. 1482–1491
2 Shamlou, S., Mirsalim, M.: 'Design, optimisation, analysis and experimental verification of a new line-start permanent magnet synchronous shaded-pole motor', *IET Electr. Power Appl.*, 2013, **7**, (1), pp. 16–26
3 Pietruszka, M., Napieralska-Juszczak, E.: 'Quasi 3D magnetic field computation for anisotropic sheet layer structure', *COMPEL*, 1995, **14**, (4), pp. 163–167
4 Gysen, B., Meessen, K., Paulides, J., Lomonova, E.: '3-D analytical and numerical modelling of tubular actuators with skewed permanent magnets', *IEEE Trans. Magn.*, 2011, **47**, (9), pp. 2200–2212
5 Demenko, A.: 'Finite element analysis of electromagnetic torque saturation harmonics in a squirrel cage machine', *COMPEL*, 1999, **18**, (4), pp. 619–628

6 Jagiela, M., Mendrela, E.A., Gottipati, P.: 'Investigation on a choice of stator slot skew angle in brushless PM machines', *Electr. Eng.*, 2013, **95**, (3), pp. 209–219
7 Demenko, A., Wojciechowski, R.M., Sykulski, J.K.: '2D versus 3D electromagnetic field modelling in electromechanical energy converters', *IEEE Trans. Magn.*, 2014, **50**, (2), pp. 1–4
8 Mahmoudi, A., Kahourzade, S., Rahim, N.A., Ping, W.H.: 'Improvement to performance of solid-rotor-ringed line-start axial-flux permanent-magnet motor', *Prog. Electromagn. Res. – PIER*, 2012, **124**, pp. 383–404
9 Lukaniszyn, M., Jagiela, M., Wrobel, R.: 'A disc-type motor with co-axial flux in the stator; -influence of magnetic circuit parameters on the torque', *Electr. Eng.*, 2002, **84**, (2), pp. 91–100
10 Demenko, A.: '3D edge element analysis of permanent magnet motor dynamics', *IEEE Trans. Magn.*, 1998, **34**, (5), pp. 3620–3623
11 Wojciechowski, R.M., Mendrela, E.A., Demenko, A.: 'Magnetic field and torque in permanent magnet slot-less brushless motor with twin cylindrical rotor', *Prz. Elektrotech.*, 2009, **85**, (12), pp. 246–251
12 Demenko, A., Sykulski, J.K.: 'Network equivalents of nodal and edge elements in electromagnetics', *IEEE Trans. Magn.*, 2002, **38**, (2), pp. 1305–1308
13 Stachowiak, D., Demenko, A.: 'Representation of permanent magnets in the 3D finite element description of electrical machines', *Electromotion*, 2007, **14**, (1), pp. 3–9
14 Wojciechowski, R.M., Jedryczka, C., Lukaszewicz, P., Kapelski, D.: 'Analysis of high speed permanent magnet motor with powder core material', *COMPEL*, 2012, **31**, (5), pp. 1528–1540
15 Demenko, A., Sykulski, J.K., Wojciechowski, R.M.: 'On the equivalence of finite element and finite integration formulations', *IEEE Trans. Magn.*, 2010, **46**, (8), pp. 3169–3172
16 Demenko, A., Stachowiak, D.: 'Electromagnetic torque calculation using magnetic network methods', *COMPEL*, 2008, **27**, (1), pp. 17–26
17 Jagiela, M., Garbiec, T.: 'Evaluation of rotor-end factors in solid-rotor induction motors', *IEEE Trans. Magn.*, 2012, **48**, (10), pp. 137–142